A Statistical Model for the Headed and Tail Distributions of Random Telegraph Signal Magnitudes in Nanoscale MOSFETs

Ming-Jer Chen, *Senior Member, IEEE*, Kong-Chiang Tu, Huan-Hsiung Wang, Chuan-Li Chen, Shiou-Yi Lai, and You-Sheng Liu

***Abstract*— Trapping-detrapping of a single electron via an individual trap in metal–oxide–semiconductor field-effect transistor (MOSFET) gate dielectric constitutes two-level random telegraph signals. Recent 3-D technology computer-aided design (TCAD) simulations, on an individual MOSFET, revealed that with the position of the trap as a random variable, resulting random telegraph signals relative magnitude $\Delta I_d/I_d$ in the subthreshold current at low drain voltage can have two distinct distributions: a headed one for a percolation-free channel and a tail one for a percolative channel. The latter may be effectively treated by a literature formula: $(\Delta I_d/I_d) = (I_{\mathrm{loc}}/I_d)^2$, where I_{loc} is the local current around the trap. In this paper, we show how to make this formula practically useful. First, we conduct 3-D TCAD simulations on a 35 × 35-nm^2 channel to provide $\Delta I_d/I_d$ for a few positions of the trap. This leads to a new statistical model in closed form, which can reproduce headed distributions. Straightforwardly, key criteria are drawn from the model, which can act as guidelines for the adequate use of the I_{loc}/I_d formula. Extension to threshold voltage shift counterparts, from subthreshold through transition to inversion, is successfully achieved. Importantly, use of the model may overcome the drawbacks of the statistical experiment or simulation in the field.**

***Index Terms*— Fluctuations, metal–oxide–semiconductor field-effect transistors (MOSFETs), nano, noise, percolation, random telegraph signals (RTSs), technology computer-aided design (TCAD), trap.**

I. Introduction

In 1984, Ralls *et al.* [1] of Bell Laboratories first observed random telegraph signals (RTSs) in metal–oxide–semiconductor field-effect transistors (MOSFETs) and had attributed such phenomena to the alternate capture and emission of a single electron at a certain individual gate dielectric trap. Since then, RTS of MOSFETs has attracted so many researchers [2]–[22] for its unique capability, relative to expensive nanometer-precision probe equipment, to examine atomic-sized traps, blocked regions, and even the underlying channel. More recently, the study in the field has substantially turned to RTS relative magnitude or equivalently the extra threshold voltage shift [23]–[26]. The reason is that state-of-the-art MOSFETs have been aggressively scaled down to the extent the RTS critically impacts, primarily through its relative magnitude as shown in Fig. 1 for a two-level RTS in the source/drain current under fixed drain and gate voltages.

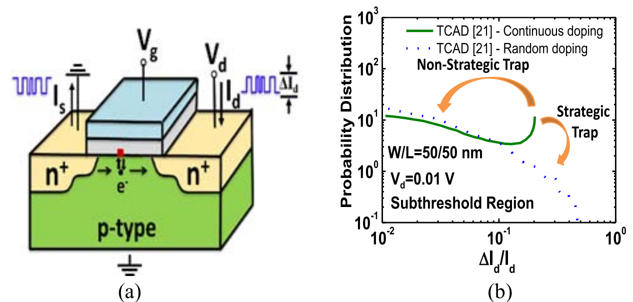

Fig. 1. (a) Schematics of a MOSFET structure showing the electron trapping-detrapping process via a trap in gate dielectric and corresponding two-level RTS in the source and drain current. (b) 3-D TCAD created statistical distributions (from 200 samples) [21] of RTS relative magnitude in the subthreshold current at low drain voltage: a headed distribution (solid line) in a percolation-free channel and a tail distribution (dotted line) in a percolative channel. The two arrows indicate the separation of the headed distribution into the tail one via the strategically located trap and the remaining via the nonstrategically located trap [18]. Note that there is an intersection between two curves.

There has been a simplest but widely quoted model for the source/drain current RTS magnitude [2], [17]

$$\frac{\Delta I_d}{I_d} = \frac{L_t^2}{WL} \tag{1}$$

where L_t is the effective size of the blocked region around the trapped electron, and W and L are the channel width and length, respectively. Relative magnitude $\Delta I_d/I_d$ corresponds to extra threshold voltage shift under constant source/drain current. Such relative current magnitudes or threshold voltage shifts have been experimentally demonstrated to have large values or significant variations, particularly for static RAM [27] and flash memory [28]. Thus, the ability to quantify $\Delta I_d/I_d$ through (1) is essential and crucial. In doing so,

Manuscript received December 18, 2013; accepted May 2, 2014. Date of publication May 29, 2014; date of current version June 17, 2014. This work was supported by the National Science Council of Taiwan under Contract NSC 100-2221-E-009-017-MY3. The review of this paper was arranged by Editor Z. Celik-Butler.

M.-J. Chen, K.-C. Tu, H.-H. Wang, C.-L. Chen, and Y.-S. Liu are with the Department of Electronics Engineering, Institute of Electronics, National Chiao Tung University, Hsinchu 300, Taiwan (e-mail: chenmj@faculty.nctu.edu.tw; kctu.ee96g@g2.nctu.edu.tw; treebeard.ee96@g2.nctu.edu.tw; recreation2266.ep97@g2.nctu.edu.tw; idoflymark@gmail.com).

S.-Y. Lai is with the Ministry of the Interior, Taipei 100, Taiwan (e-mail: lineage78225@hotmail.com).

Color versions of one or more of the figures in this paper are available online at http://ieeexplore.ieee.org.

Digital Object Identifier 10.1109/TED.2014.2323259

0018-9383 © 2014 IEEE. Translations and content mining are permitted for academic research only. Personal use is also permitted, but republication/redistribution requires IEEE permission. See http://www.ieee.org/publications_standards/publications/rights/index.html for more information.

one must take into account the two key factors. First, different positions of the RTS responsible trap correspond to different values of $\Delta I_d/I_d$ and therefore, with the position of the trap being actually unknown, the context of probability and statistics is needed to treat the underlying $\Delta I_d/I_d$. Second, there is a percolative nature in the channel, due to random fixed charges [18] and/or random discrete dopants [29].

To resolve this, one may have two ways. The first way goes to 2-D technology computer-aided design (TCAD) simulations [18], 3-D TCAD simulations [21], [24]–[26], or 3-D analytical models [23], each with its own percolation paths. Specifically, simulations by Asenov *et al.* [21], on an individual 50×50 nm^2 MOSFET in the subthreshold region at low drain voltage, pointed to the existence of the two different distributions of $\Delta I_d/I_d$, as shown in Fig. 1(b): a headed and a tail distribution. The former is due to the uncertainty in the trap position, in case of no percolation, whereas the presence of the percolation gives rise to the latter having an extended range to higher $\Delta I_d/I_d$. As illustrated in the figure (see more detailed explanations later), once the strategically located traps are involved [18], part of the headed distribution will fall down and become the tail one.

The second way goes to (1) again, especially its statistical version. According to [18], the following relationship can be derived from (1):

$$\frac{\Delta I_d}{I_d} = \left(\frac{I_{\text{loc}}}{I_d}\right)^2 \tag{2}$$

where I_{loc} represents the local current around the trap. The ratio of the local current to the total current, I_{loc}/I_d, was experimentally found to follow a normal distribution, denoted as $n_0(I_{\text{loc}}/I_d)$ [18]. Consequently, the distribution function of $\Delta I_d/I_d$, $h(\Delta I_d/I_d)$, can be obtained by performing the function transformation on (2) [18]

$$h\left(\frac{\Delta I_d}{I_d}\right) = n_0\left(\frac{I_{\text{loc}}}{I_d}\right)\left(\frac{\Delta I_d}{I_d}\right)^{-1/2} \Big/ 2. \tag{3}$$

The application of (3) had successfully reproduced the experimental tail distribution of $\Delta I_d/I_d$ from an ensemble of 187 samples of 500×500 nm^2 MOSFETs, all operated in the subthreshold region [18]. Corresponding mean m_{loc} and standard deviation σ_{loc} of the normal variable I_{loc}/I_d reflects the underlying individual percolation path due to the use of the same manufacturing process [18]. In principle, different sets of m_{loc} and σ_{loc} correspond to different manufacturing processes and hence different percolation paths, and vice versa (the validity of this statement will be examined in the subsequent sections). However, several issues concerning the use of (3) arise, due to the uncertainties in m_{loc} and σ_{loc}. First, it is unclear whether m_{loc} or σ_{loc} is unlimited. Second, the values of m_{loc} and σ_{loc} are unique or not, if they are extracted from a given percolative channel. Third, m_{loc} and σ_{loc} should change or not, if the operating conditions change. Finally, guidelines to adequately determine m_{loc} and σ_{loc} were lacking to date. Only with these issues clarified and resolved can the practical application of (3) be possible.

At this point, one should keep in mind that there exist fundamental limitations associated with the statistical experiment [18] and statistical TCAD 3-D simulation [21], [24]–[26]. First, the statistical sample size used (e.g., 187 trap positions in the statistical experiment [18]; and 200 and 300 trap positions in the 3-D TCAD simulation [21] and [25], respectively) may not be large enough to make the created tail distributions statistically meaningful. Second, the measurement equipment is usually featured by such specifications as precisions; and the TCAD simulation result depends considerably on the numerical error (i.e., the convergence error or the size of the mesh in structure). The measurement precision or numerical error is likely to limit the visible range of the created distribution. These drawbacks may all be overcome if one turns to the use of (3).

In this paper, we show how to make (3) practically useful. First, we focus on a 35×35-nm^2 MOSFET and limit the operating conditions to the subthreshold regime at low drain voltage (0.05 V). To achieve the goal efficiently, we make use of a commercially available 3-D TCAD simulation tool and execute it only for several trap positions in case of no percolation. This leads to the statistical version of (1) in closed form, which can reproduce headed distributions well. Straightforwardly, it enables the establishment of the key criteria and hence the guidelines to ensure the adequate use of (3) in percolation conditions. Resulting tail distributions are validated. Aforementioned issues associated with m_{loc} and σ_{loc} are also made clear. Extension to RTS-induced threshold voltage shift, in a wide range of gate voltages from subthreshold to inversion, is done as well.

II. Percolation Free Channel: Model and Validation

3-D TCAD Sentaurus [30], in its default conditions (i.e., the conventional scattering mechanisms due to ionized impurity atoms, phonons, and surface roughness; and the density gradient model for the quantum confinement), was employed. Simulation structure is a bulk n-channel $W/L = 35/35$-nm MOSFET structure (with no shallow trench isolation (STI); the effect of including the STI as in [31] and [32] will be addressed later) with the equivalent gate oxide thickness of 2 nm and p-type substrate doping concentration of 2×10^{18} cm^{-3} (continuous doping, with no halo implants). Simulated subthreshold I–V characteristic is shown in Fig. 2(a). Corresponding threshold voltage and subthreshold swing (SS) are labeled. A negatively charged trap was placed at the SiO_2/Si interface to simulate the altered drain current. TCAD was carried out, with different positions of such trap along the transport direction but fixed at the midchannel (those fixed at the edge part will be discussed later) in the width direction. Simulated $\Delta I_d/I_d$ at $V_g = 0$ is shown in Fig. 2(b) versus the distance d of the trap from the midchannel in the transport direction. Corresponding L_t as extracted by (1) is added to the figure. Evidently, the maximum $\Delta I_d/I_d$ and L_t correspond to the midchannel trap and will decrease with increasing distance from midchannel; and owing to the symmetry of the structure in the channel length direction, which is valid only for small enough drain voltage, it can be inferred that the same distance will have the same $\Delta I_d/I_d$, regardless of the trap located

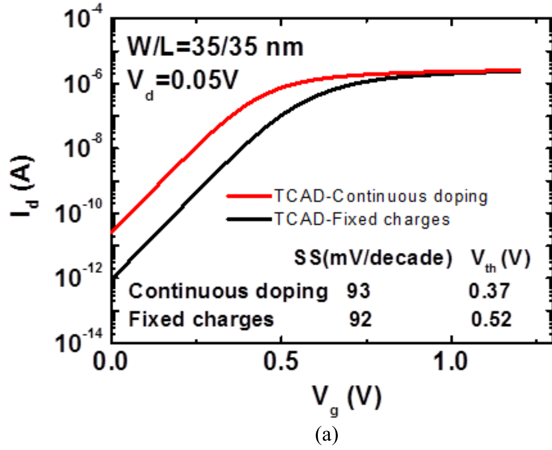

(a)

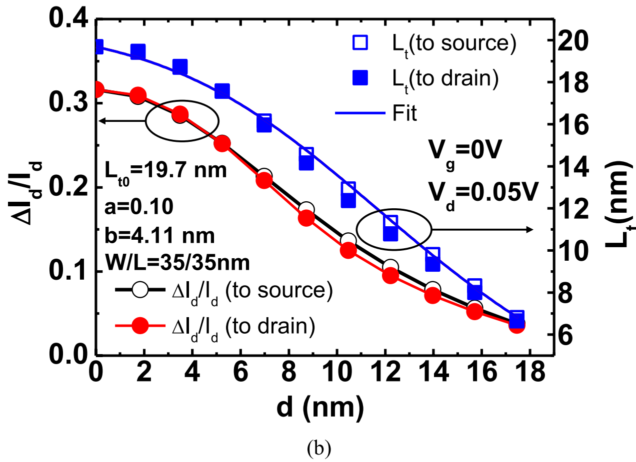

(b)

Fig. 2. (a) Simulated subthreshold I–V characteristics with (black line) and without (red line) percolation. Corresponding SS and threshold voltage are labeled. (b) Simulated $\Delta I_d/I_d$ and corresponding L_t (empty symbols for traps between midchannel and source; solid symbols for traps between midchannel and drain) versus the distance d from the midchannel. Fitting line via (4) yields L_{t0} = 19.7 nm, a = 0.10, and b = 4.11 nm.

near source or drain. Furthermore, we suggest that $\Delta I_d/I_d$ is appropriately a weak function of the trap position in the width direction (the reasons will be given later, along with the STI issue). Similar statements were also reported in case of W/L = 50/50 nm (with no STI) [21].

There are many empirical formulas one can use to fit L_t in Fig. 2(b). Here, we adopted the following one, without any particular reason:

$$L_t = \frac{L_{t0}}{\sqrt{1 + a(\exp(d/b) - 1)}}. \tag{4}$$

Data fitting yields L_{t0} = 19.7 nm, a = 0.10, and b = 4.11 nm. The fitting quality is good, meaning that only a few trap positions, but with enough distance between positions, are needed in the simulation. This greatly reduces the computational load in the 3-D TCAD simulation. Note that L_{t0} stands for L_t in case of midchannel trap ($d = 0$). Then, it is a straightforward task to derive a closed-form statistical model for $\Delta I_d/I_d$. The derivation process is shown in Fig. 3. First, we can reasonably assume that: 1) the probability of finding a region between midchannel and source is 1/2, equal to that of the remaining between midchannel and drain and 2) the probability of finding

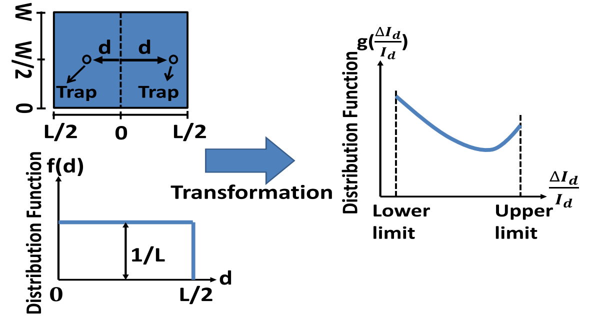

Fig. 3. Derivation process for the statistical model of the RTS source/drain current magnitude in the percolation free case.

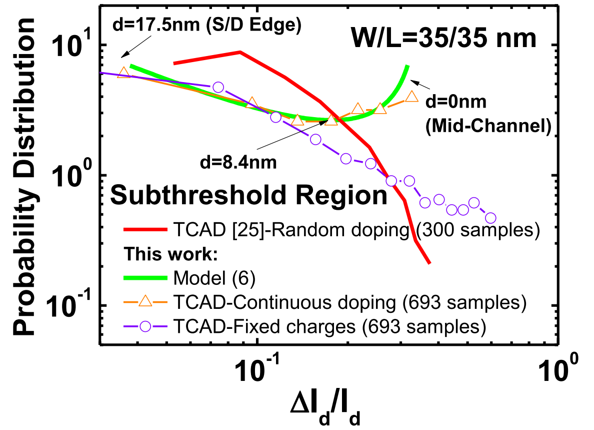

Fig. 4. Calculated (green solid line) and simulated (yellow line with triangle) $\Delta I_d/I_d$ headed distributions in this paper for the percolation free case. Together plotted are simulated tail distributions due to fixed charges in this paper (V_d = 0.05 V) and due to random discrete dopants from the citation (V_d = 0.01 V) [25]. Corresponding sample size (i.e., number of the trap positions) is given. In this paper, V_g = 0 and V_d = 0.05 V.

a trap at a certain d is constant across the channel. Thus, the distribution function of the trap distance d ($0 \leq d \leq L/2$) in each of these two regions can read as

$$f(d) = \frac{1}{L}. \tag{5}$$

Next, by substituting (4) into (1) and applying the function transformation to (5), the distribution function of $\Delta I_d/I_d$ can result

$$g\left(\frac{\Delta I_d}{I_d}\right) = 2bf(d)\left(1 + \frac{1-a}{a}\exp\left(-\frac{d}{b}\right)\right) \Big/ \frac{\Delta I_d}{I_d}. \tag{6}$$

The upper and lower limits of $\Delta I_d/I_d$ correspond to $d = 0$ and $L/2$, respectively, both of which can be readily calculated. The area under the distribution curve created by (6) between lower and upper limits is equal to unity.

Calculated distribution function of $\Delta I_d/I_d$ appears to pile up near the upper limit of $\Delta I_d/I_d$, typical of the headed distribution, as shown in Fig. 4. To testify to the validity of the model and its assumptions, we add to the figure a TCAD created distribution curve in this paper, with a large sample size of 693 (i.e., 693 TCAD simulation structures with only one trap randomly positioned across the whole channel). Fairly good agreements between the two are evident, achieved

without adjusting any parameters in model or simulation in this paper. Therefore, the ability of the devised statistical model to reproduce headed distributions is verified.

III. Percolative Channel: Criteria and Guidelines

Key criteria for percolation case can be drawn from the calculated headed distribution via (6). First, in the so-called subthreshold region of operation, there are specific regions near source and drain, away from the midchannel, where the electron concentration is much larger than that around midchannel. This means that the strong inversion dominates in these local regions. In other words, the subthreshold region of operation strictly applies only to around the midchannel. Such localized strong inversion near source and drain junctions holds even in the percolation case, as earlier mentioned in [21]. In a sense, the percolation effect in such local strong-inversion regions should be greatly reduced, due to enhanced electron screening. Two extra sources of corroborative evidence exist. First, in [33], subthreshold current mismatch significantly decreases as the electron density increases via a substrate forward bias. Second, 3-D TCAD simulation results [24] suggested that the closer to source or drain the trap is situated, the lower the corresponding RTS-induced threshold voltage shift.

Thus, the first key criterion emerges: the $\Delta I_d/I_d$ distribution curve near the lower limit does not change too much between the two cases of with and without percolation. In other words, the lower $\Delta I_d/I_d$ distribution in the presence of the percolation is considerably close to that of the headed one. This also means that the lower limit of I_{loc}/I_d can reasonably be set by the lower limit of $\Delta I_d/I_d$ with $d = L/2$. In a sense, the normal distribution function of I_{loc}/I_d in (3) must be modified as the limiting one

$$n\left(\frac{I_{\text{loc}}}{I_d}\right) = \frac{n_0\left(\frac{I_{\text{loc}}}{I_d}\right)}{\int_{\left(I_{\text{loc}}/I_d\right)_{\min}}^{\left(I_{\text{loc}}/I_d\right)_{\max}} n_0\left(\frac{I_{\text{loc}}}{I_d}\right) d\frac{I_{\text{loc}}}{I_d}} \quad (7)$$

where $n_0(I_{\text{loc}}/I_d)$ is the standard (unlimited) normal distribution function with the mean m_{loc} and standard deviation σ_{loc}, $(I_{\text{loc}}/I_d)_{\min}$ is the squared root of the lower limit of $\Delta I_d/I_d$ in the headed distribution, and $(I_{\text{loc}}/I_d)_{\max}$ is set at 1 to reflect the worst case conditions (i.e., RTS high level being I_d and low level zero).

The second is related to the remaining region around the midchannel. In this region, there are, to a first-order approximation, two types of individual traps responsible for RTS: one of the strategically located trap and one of the nonstrategic trap [18]. The former is likely to produce a value of $\Delta I_d/I_d$ larger than that of the upper limit of the headed distribution and hence constitute the tail distribution at higher $\Delta I_d/I_d$. As for the latter, its role is simply to raise the resulting distribution curve near lower limit to above that of no percolation. Thus, part of the headed distribution near the upper limit is repopulated and separated into two different components in percolation case: 1) higher $\Delta I_d/I_d$ part and 2) lower $\Delta I_d/I_d$ part [Fig. 1(b)]. Because the area under the distribution curve is unity, the distribution curve in the presence of the percolation must intersect with that of no percolation. Thus, the required intersection between the two curves may serve as the second criterion.

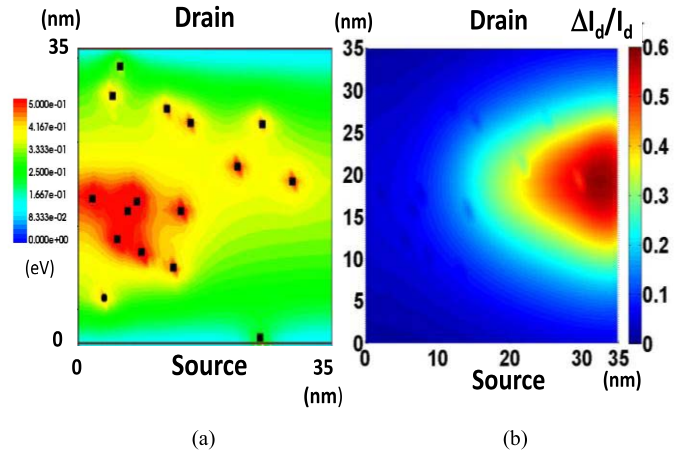

Fig. 5. (a) Simulated conduction-band energy on 35 × 35-nm^2 channel in the presence of fixed charges (black squares) and (b) corresponding $\Delta I_d/I_d$ distributions (created from 693 trap positions). The number of fixed charges is 16 and hence the average density is 1.3 × 10^{12} cm^{-2}. $V_g = 0$ and $V_d = 0.05$ V.

To support those criteria, we added a percolation path to the TCAD simulation structure in terms of the negatively fixed charges, following the approach in [18]. The number of fixed charges in this paper is 16 and hence the average density of fixed charges is 1.3 × 10^{12} cm^{-2}. Simulated I–V and potential distribution over channel are shown in Figs. 2(a) and 5(a), respectively. Different positions of the trap (693 positions) correspond to different simulated $\Delta I_d/I_d$ values, thus producing a map of $\Delta I_d/I_d$ as together shown in Fig. 5(b). These trap-position-dependent $\Delta I_d/I_d$ distributions are quite smooth, due to the very short distance from position to position. Corresponding $\Delta I_d/I_d$ distribution curve is added to Fig. 4.

Evidently, our TCAD simulated $\Delta I_d/I_d$ distribution curve due to fixed charges intersects with that of no such fixed charges, with the two following features newly created: 1) part of its distribution near the lower $\Delta I_d/I_d$ limit is slightly higher than no percolation and 2) a tail distribution appears at higher $\Delta I_d/I_d$ than the upper limit of headed distribution. Our simulation results resemble those of 50/50 nm by Asenov *et al.* [21] [Fig. 1(b)], despite different percolation origins between the two. However, to make the comparison fair, we further quoted one of their simulated ones under the same channel dimension [25], as shown in Fig. 4. Once again, the intersection with the headed curve remains. Note that our TCAD simulated $\Delta I_d/I_d$ has a wider tail distribution to a maximum value of around 60%, higher than that (40%) of the citation [25]. Such difference may be attributed to the two factors: 1) more strategic traps in this paper and 2) larger sample size in this paper (see the labels in Fig. 4).

Therefore, these key criteria considerably act as guidelines through (7) in the use of (3). To illustrate this, we show in

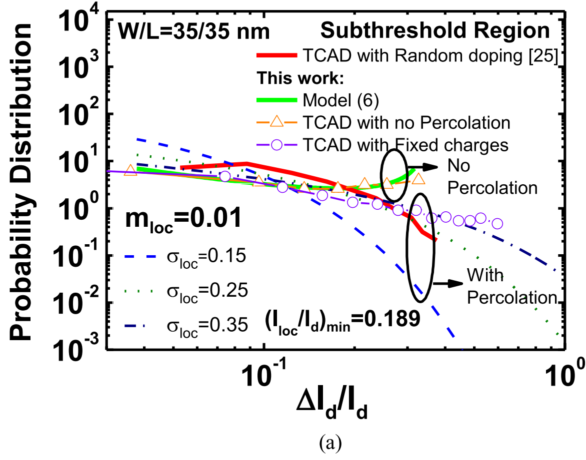

(a)

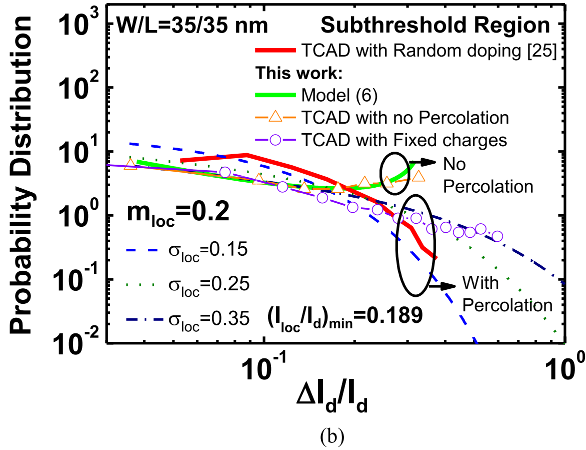

(b)

Fig. 6. Calculated $\Delta I_d/I_d$ headed and tail distribution curves. $L_{t0} = 19.7$ nm, $a = 0.10$, and $b = 4.11$ nm. (a) $m_{\text{loc}} = 0.01$ and (b) $m_{\text{loc}} = 0.2$, with σ_{loc} as a parameter. TCAD created distributions from this paper and the literature ($V_d = 0.01$ V) [25] are shown for comparison. In this paper, $V_g = 0$ and $V_d = 0.05$ V.

Fig. 6 the calculated results, for two different values of m_{loc} with σ_{loc} as a parameter. It can be seen that the distribution curve rotates clockwise as m_{loc} decreases, thus increasing the probability of intersecting with the headed one. This is the case for decreasing σ_{loc}. Such rotational change is simply to make the area under the resulting curve remain of unity. Thus, for all σ_{loc} illustrated, the condition of $m_{\text{loc}} = 0.01$ satisfies the criteria; however, as m_{loc} is increased to 0.2, only σ_{loc} of less than 0.35 can have the expected intersection. Extra works were done, leading to a critical σ_{loc} versus m_{loc} curve below which the curve intersection occurs, as shown in Fig. 7. Obviously, m_{loc} and σ_{loc} are not unlimited. Specifically, simulated tail distribution due to fixed charges in this paper can be reproduced with σ_{loc} of 0.35 for $m_{\text{loc}} = 0.01$ and σ_{loc} of 0.25 to 0.35 for $m_{\text{loc}} = 0.2$. This indicates that: 1) the extracted m_{loc} and σ_{loc} from a percolation channel are not unique and 2) the tail distribution of the percolation channel can be reproduced from a few critical m_{loc} and σ_{loc}. Next, for the case of random discrete dopants [25], the optimum σ_{loc} at $m_{\text{loc}} = 0.2$ is 0.15 [Fig. 6(b)], which is less than fixed charges ones. Thus, different percolation origins and/or paths can have different combinations of m_{loc} and σ_{loc}. Further fitting to

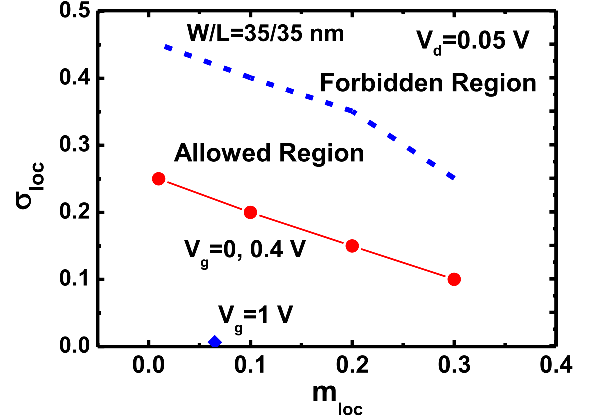

Fig. 7. Plot of a critical σ_{loc} versus m_{loc} curve as drawn from the works, as in Fig. 6. Only for sets of σ_{loc} and m_{loc} lying below the curve, the calculated tail distribution can have intersections with the headed distribution. Extracted σ_{loc} and m_{loc} from the tail distributions for three gate voltages [25] appear, as expected, in the allowed region.

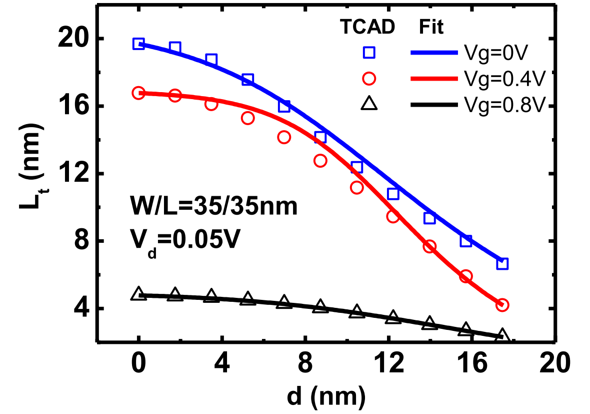

Fig. 8. Symbols: extracted L_t versus the trap distance at three gate voltages. Fitting lines using (4) are shown. Corresponding model parameters are: 1) $L_{t0} = 19.7$ nm, $a = 0.10$, and $b = 4.11$ nm for $V_g = 0$; 2) $L_{t0} = 16.7$ nm, $a = 0.02$, and $b = 2.57$ nm for $V_g = 0.4$ V; and 3) $L_{t0} = 4.7$ nm, $a = 0.07$, and $b = 4.50$ nm for $V_g = 0.8$ V.

other tail distributions [25] was done concerning the effect of gate voltage. We found that extracted m_{loc} and σ_{loc} have significantly low values, if the gate voltage is large enough, as shown in Fig. 7.

IV. Extension and Discussion

We further extend the work to RTS-induced threshold voltage shift, at three gate voltages: $V_g = 0$, 0.4, and 0.8 V. Since the threshold voltage is 0.37 or 0.52 V [Fig. 2(a)], these three gate voltages separately represent the subthreshold, transition, and inversion region of operation. Corresponding $\Delta I_d/I_d$ magnitudes in the percolation free channel had been simulated by 3-D TCAD, leading to L_t in Fig. 8 as a function of the trap distance. The figure clearly reveals that the maximum L_t stems from midchannel traps ($d = 0$), valid for all gate voltages illustrated. Increasing gate voltage produces a decrease in L_t, as expected due to increased electron screening. This strongly corroborates the applicability of (4) and hence the statistical model (6) in the transition and above-threshold region.

Again through data fitting, three model parameters, L_{t0}, a, and b had been extracted: 1) $L_{t0} = 19.7$ nm, $a = 0.10$, and $b = 4.11$ nm for $V_g = 0$; 2) $L_{t0} = 16.7$ nm, $a = 0.02$, and $b = 2.57$ nm for $V_g = 0.4$ V; and 3) $L_{t0} = 4.7$ nm, $a = 0.07$, and $b = 4.50$ nm for $V_g = 0.8$ V. Substituting these values into (6), we obtained headed distributions of $\Delta I_d/I_d$. Corresponding threshold voltage shift ΔV_{th} distributions were readily determined using the two transformation formulas. One is the SS method [34]

$$\Delta V_{\text{th}} = -\frac{SS}{\ln 10}\ln\left(1-\frac{\Delta I_d}{I_d}\right). \tag{8}$$

Using the function transformation, one can reach the distribution function for the threshold voltage shift

$$l(\Delta V_{\text{th}}) = g\left(\frac{\Delta I_d}{I_d}\right)\frac{\ln 10}{SS}\exp\left(-\frac{\Delta V_{\text{th}}}{SS}\ln 10\right). \tag{9}$$

The other is the transconductance method [34] for the inversion case

$$\Delta V_{\text{th}} = (V_g - V_{\text{th}})\frac{\Delta I_d}{I_d}. \tag{10}$$

Since the gate overdrive $(V_g - V_{\text{th}})$ is constant, the transformed ΔV_{th} distribution is the $\Delta I_d/I_d$ distribution times this constant.

Resulting ΔV_{th} distributions are given in Fig. 9, all featuring headed ones. We found that ΔV_{th} distributions from both transformation methods are almost the same at $V_g = 0.4$ V, the transition region between subthreshold and inversion. In Fig. 9, we add the simulated ΔV_{th} distribution curves due to random discrete dopants as quoted from the same source [25]. Again, the intersection with the headed curve appears in case of RTS-induced threshold voltage shift, in a wide range of gate voltages. Next, we combine the I_{loc}/I_d statistical model [(3) with (7) incorporated] with the $\Delta I_d/I_d$ to ΔV_{th} transformation formulas, to reproduce ΔV_{th} tail distributions. In the beginning, we fixed m_{loc} and σ_{loc} at the optimum set ($m_{\text{loc}} = 0.2$ and $\sigma_{\text{loc}} = 0.15$), as mentioned in the preceding section for the same random discrete dopants. Calculated ΔV_{th} distributions are shown to be comparable with those simulated with the random discrete dopants in channel [25], but only valid at $V_g = 0$ and 0.4 V. Serious discrepancies take place, as V_g increases to 0.8 V. We found that both m_{loc} and σ_{loc} must be reduced in this inversion regime. With the new values of $m_{\text{loc}} = 0.05$ and $\sigma_{\text{loc}} = 0.05$, reasonable reproduction is achieved. Such change in m_{loc} and σ_{loc} supports those of arguments by Asenov *et al.* [21] from their simulation task that underlying percolation paths will electrically change, when the operating conditions change. Extra evidence exists. In [22], experimentally extracted percolation coefficients undergo significant change from subthreshold to inversion.

More recently, Asenov's group published their works on the impact of including STI in the simulation structure [31], [32]. Relatively, such STI substructure was lacking in this paper; but essentially, this can be compensated by adding a delta width, according to [35] and [36]. In this sense, extra TCAD simulation is needed to accommodate the increased effective width and hence the corresponding headed distribution can be expected in the percolation free channel. Ironically, we should focus on the width effect, especially the edge part in this paper.

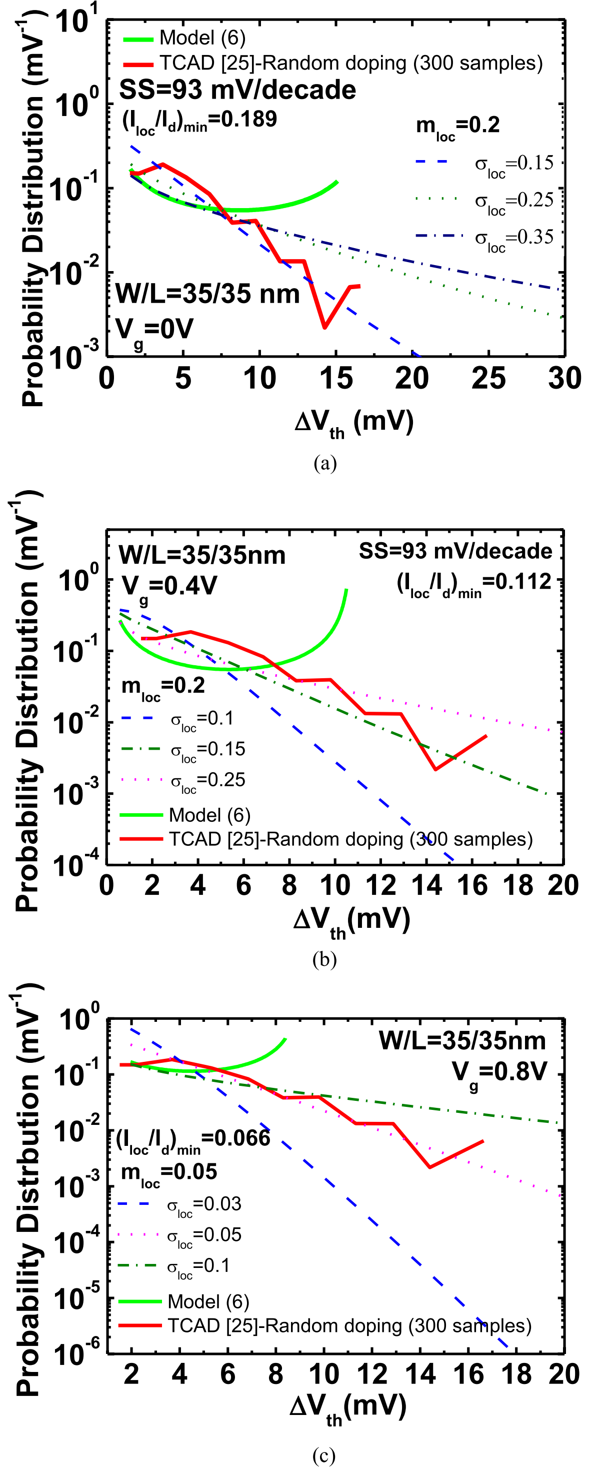

Fig. 9. Calculated ΔV_{th} (green solid lines) headed and (nonsolid lines) tail distribution curves at (a) $V_g = 0$, (b) $V_g = 0.4$ V, and (c) $V_g = 0.8$ V. Simulated (red solid lines) tail distributions due to random discrete dopants [25] are shown, along with calculated ones from several values of m_{loc} and σ_{loc}. Clearly, m_{loc} and σ_{loc} both must be reduced while entering into inversion regime, indicating that the underlying percolation paths electrically change, as well known in the field. $V_d = 0.05$ V in this paper.

Fig. 10 shows the simulated potential and $\Delta I_d/I_d$ distribution over channel in the absence of the percolation. It can be seen that potential is uniform from edge to edge in the width

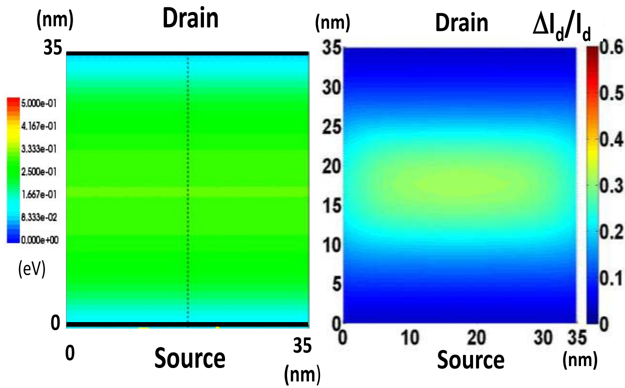

Fig. 10. Simulated potential and $\Delta I_d/I_d$ distribution over channel corresponding to the headed distribution in Fig. 4.

direction, whereas $\Delta I_d/I_d$ values near both edges are much smaller than the remaining region around the midchannel. Such region of smaller $\Delta I_d/I_d$ is very limited, thus contributing insignificantly to the TCAD simulated headed distribution in this paper. More importantly, such edge effect may further be weakened if the delta width is incorporated.

Furthermore, we want to stress that the model derivation procedure can handle the large drain voltage conditions. First, corresponding trap distance dependencies [21], [26] differ significantly from those of low drain voltage as in this paper. Even such situations are likely to occur for device with halo implant or nonuniform doping in the channel, which were not particularly included in this paper. Thus, the empirical formula used in this paper for L_t, (4), might fail and is better replaced with other more suitable ones. Nevertheless, the presented model derivation and function transformation essentially holds and key criteria and guidelines can further be reached as well.

Finally, we summarize the merits of the proposed statistical model as follows.

1) It needs only a few trap positions in the 3-D TCAD percolation-free simulation (or an analytical 3-D I–V model without using any 3-D TCAD tools), without doing too much in this numerically demanding process.
2) It can efficiently create headed $\Delta I_d/I_d$ and ΔV_{th} distributions and thereby criteria and guidelines for the tail distributions.
3) It can effectively overcome the limitations of the statistical experiment or 3-D simulation in the field, such as the limited sample size, the numerical error, the measurement precision, the unrefined mesh, and even the extraordinarily huge CPU time.

V. Conclusion

The closed-form statistical model has been devised and has reproduced headed distributions of two-level RTS magnitudes in the subthreshold current at low drain voltage. Key criteria have been drawn and guidelines have therefore been created to enable the adequate use of the literature I_{loc}/I_d formula in percolation case. Resulting tail distributions have shown to be in agreement with those obtained from 3-D TCAD simulations. Extension to threshold voltage shift counterparts has satisfactorily been done. Effect of varying gate voltage from subthreshold to inversion on the underlying percolation path, through the two key parameters (mean and standard deviation) of I_{loc}/I_d, has been explicitly examined. Other issues such as width dependence, large drain voltage, and nonuniform doping have been addressed. Merits of the model proposal have been summarized.

References

[1] K. S. Ralls *et al.*, "Discrete resistance switching in submicrometer silicon inversion layers: Individual interface traps and low-frequency ($1/f$?) noise," *Phys. Rev. Lett.*, vol. 52, no. 3, pp. 228–231, Jan. 1984.
[2] M. J. Kirton and M. J. Uren, "Noise in solid-state microstructures: A new perspective on individual defects, interface states and low-frequency ($1/f$) noise," *Adv. Phys.*, vol. 38, no. 4, pp. 367–468, Jul. 1989.
[3] M. J. Chen and M. P. Lu, "Electrically probing atomic-sized oxide traps," in *Encyclopedia of Nanoscience and Nanotechnology*, vol. 13, H. S. Nalwa, Ed. Valencia, CA, USA: American Scientific Publishers, 2011, pp. 243–261.
[4] K. K. Hung, P. K. Ko, C. Hu, and Y. C. Cheng, "Random telegraph noise of deep-submicrometer MOSFETs," *IEEE Electron Device Lett.*, vol. 11, no. 2, pp. 90–92, Feb. 1990.
[5] M. Schulz, "Coulomb energy of traps in semiconductor space-charge regions," *J. Appl. Phys.*, vol. 74, no. 4, pp. 2649–2657, Aug. 1993.
[6] H. H. Mueller, D. Wörle, and M. Schulz, "Evaluation of the Coulomb energy for single-electron interface trapping in sub-μm metal-oxide-semiconductor field-effect transistors," *J. Appl. Phys.*, vol. 75, no. 6, pp. 2970–2979, Mar. 1994.
[7] A. Palma, A. Godoy, J. A. Jiménez-Tejada, J. E. Carceller, and J. A. López-Villanueva, "Quantum two-dimensional calculation of time constants of random telegraph signals in metal–oxide–semiconductor structures," *Phys. Rev. B*, vol. 56, no. 15, pp. 9565–9574, Oct. 1997.
[8] Z. Celik-Butler and F. Wang, "Effects of quantization on random telegraph signals observed in deep-submicron MOSFETs," *Microelectron. Rel.*, vol. 40, no. 11, pp. 1823–1831, 2000.
[9] M. Xiao, I. Martin, and H. W. Jiang, "Probing the spin state of a single electron trap by random telegraph signal," *Phys. Rev. Lett.*, vol. 91, no. 7, p. 078301, Aug. 2003.
[10] M.-P. Lu and M.-J. Chen, "Oxide-trap-enhanced Coulomb energy in a metal-oxide-semiconductor system," *Phys. Rev. B*, vol. 72, no. 23, p. 235417, Dec. 2005.
[11] J.-W. Lee, B. H. Lee, H. Shin, and J.-H. Lee, "Investigation of random telegraph noise in gate-induced drain leakage and gate edge direct tunneling currents of high-κ MOSFETs," *IEEE Trans. Electron Devices*, vol. 57, no. 4, pp. 913–918, Apr. 2010.
[12] H.-J. Cho *et al.*, "Investigation of gate etch damage at metal/high-κ gate dielectric stack through random telegraph noise in gate edge direct tunneling current," *IEEE Electron Device Lett.*, vol. 32, no. 4, pp. 569–571, Apr. 2011.
[13] B. Oh *et al.*, "Characterization of an oxide trap leading to random telegraph noise in gate-induced drain leakage current of DRAM cell transistors," *IEEE Trans. Electron Devices*, vol. 58, no. 6, pp. 1741–1747, Jun. 2011.
[14] W. Goes, F. Schanovsky, T. Grasser, H. Reisinger, and B. Kaczer, "Advanced modeling of oxide defects for random telegraph noise," in *Proc. 21st ICNF*, Jun. 2011, pp. 204–207.
[15] I.-O. Yoon, S. Choi, S. Rhee, H. Kim, S. Park, and Y. J. Park, "Correction of the RTN model considering 3D effect of single trapped charge," in *Proc. SISPAD*, Sep. 2012, pp. 412–415.
[16] S.-W. Yoo, Y. Son, and H. Shin, "Capture cross section of traps causing random telegraph noise in gate-induced drain leakage current," *IEEE Trans. Electron Devices*, vol. 60, no. 3, pp. 1268–1271, Mar. 2013.
[17] E. Simoen, B. Dierickx, C. L. Claeys, and G. J. Declerck, "Explaining the amplitude of RTS noise in submicrometer MOSFETs," *IEEE Trans. Electron Devices*, vol. 39, no. 2, pp. 422–429, Feb. 1992.
[18] H. H. Mueller and M. Schulz, "Random telegraph signal: An atomic probe of the local current in field-effect transistors," *J. Appl. Phys.*, vol. 83, no. 3, pp. 1734–1741, Feb. 1998.
[19] A. Avellan, W. Krautschneider, and S. Schwantes, "Observation and modeling of random telegraph signals in the gate and drain currents of tunneling metal–oxide–semiconductor field-effect transistors," *Appl. Phys. Lett.*, vol. 78, no. 18, pp. 2790–2792, Apr. 2001.

[20] M.-J. Chen and M.-P. Lu, "On–off switching of edge direct tunneling currents in metal-oxide-semiconductor field-effect transistors," *Appl. Phys. Lett.*, vol. 81, no. 18, pp. 3488–3490, Oct. 2002.
[21] A. Asenov, R. Balasubramaniam, A. R. Brown, and J. H. Davies, "RTS amplitudes in decananometer MOSFETs: 3-D simulation study," *IEEE Trans. Electron Devices*, vol. 50, no. 3, pp. 839–845, Mar. 2003.
[22] M.-J. Chen, C.-C. Lee, and M.-P. Lu, "Probing a nonuniform two-dimensional electron gas with random telegraph signals," *J. Appl. Phys.*, vol. 103, no. 3, p. 034511, Feb. 2008.
[23] K. Sonoda, K. Ishikawa, T. Eimori, and O. Tsuchiya, "Discrete dopant effects on statistical variation of random telegraph signal magnitude," *IEEE Trans. Electron Devices*, vol. 54, no. 8, pp. 1918–1925, Aug. 2007.
[24] A. Ghetti, C. M. Compagnoni, A. S. Spinelli, and A. Visconti, "Comprehensive analysis of random telegraph noise instability and its scaling in deca–nanometer flash memories," *IEEE Trans. Electron Devices*, vol. 56, no. 8, pp. 1746–1752, Aug. 2009.
[25] M. F. Bukhori, S. Roy, and A. Asenov, "Simulation of statistical aspects of charge trapping and related degradation in bulk MOSFETs in the presence of random discrete dopants," *IEEE Trans. Electron Devices*, vol. 57, no. 4, pp. 795–803, Apr. 2010.
[26] N. Ashraf and D. Vasileska, "Static analysis of random telegraph noise in a 45-nm channel length conventional MOSFET device: Threshold voltage and on-current fluctuations," *IEEE Trans. Nanotechnol.*, vol. 10, no. 6, pp. 1394–1400, Nov. 2011.
[27] M. Agnostinelli *et al.*, "Erratic fluctuations of SRAM cache Vmin at the 90 nm process technology node," in *IEEE IEDM Tech. Dig.*, Dec. 2005, pp. 655–658.
[28] H. Kurata *et al.*, "The impact of random telegraph signals on the scaling of multilevel flash memories," in *Symp. VLSI Circuits, Dig. Tech. Papers*, 2006, pp. 112–113.
[29] R. W. Keyes, "The effect of randomness in the distribution of impurity atoms on FET thresholds," *Appl. Phys.*, vol. 8, no. 3, pp. 251–259, 1975.
[30] *TCAD Sentaurus, version G-2012.06*, Synopsys, Mountain View, CA, USA, 2012.
[31] X. Wang, S. Roy, A. R. Brown, and A. Asenov, "Impact of STI on statistical variability and reliability of decananometer MOSFETs," *IEEE Electron Device Lett.*, vol. 32, no. 4, pp. 479–481, Apr. 2011.
[32] S. M. Amoroso, A. Ghetti, A. R. Brown, A. Mauri, C. M. Compagnoni, and A. Asenov, "Impact of cell shape on random telegraph noise in decananometer flash memories," *IEEE Trans. Electron Devices*, vol. 59, no. 10, pp. 2774–2779, Oct. 2012.
[33] M.-J. Chen, J.-S. Ho, and T.-H. Huang, "Dependence of current match on back-gate bias in weakly inverted MOS transistors and its modeling," *IEEE J. Solid-State Circuits*, vol. 31, no. 2, pp. 259–262, Feb. 1996.
[34] J. Franco *et al.*, "BTI reliability of ultra-thin EOT MOSFETs for sub-threshold logic," *Microelectron. Rel.*, vol. 52, nos. 9–10, pp. 1932–1935, Jul. 2012.
[35] C.-Y. Hsieh, Y.-T. Lin, and M.-J. Chen, "Distinguishing between STI stress and delta width in gate direct tunneling current of narrow n-MOSFETs," *IEEE Electron Device Lett.*, vol. 30, no. 5, pp. 529–531, May 2009.
[36] C.-Y. Hsu *et al.*, "Enhanced hole mobility in non-(001) oriented sidewall corner of Si pMOSFETs formed on (001) substrate," in *Proc. IEEE SNW*, Jun. 2010, pp. 67–68.

Ming-Jer Chen (S'78–M'79–SM'98) received the Ph.D. degree from National Chiao Tung University (NCTU), Hsinchu, Taiwan, in 1985.

He has been a Professor with the Department of Electronics Engineering, NCTU, since 1985. He has supervised 20 Ph.D. and more than 100 M.S. students, all in the area of device physics.

Dr. Chen is a member of the Phi Tau Phi.

Kong-Chiang Tu received the M.S. degree in electronics engineering from the National Chiao Tung University, Hsinchu, Taiwan, in 2005, where he is currently pursuing the Ph.D. degree with the Department of Electronics Engineering, Institute of Electronics.

Huan-Hsiung Wang received the B.S. degree in electronics engineering from the National Chiao Tung University, Hsinchu, Taiwan, in 2011, where he is currently pursuing the M.S. degree with the Department of Electronics Engineering, Institute of Electronics.

Chuan-Li Chen received the B.S. degree in electrophysics from the National Chiao Tung University, Hsinchu, Taiwan, in 2012, where he is currently pursuing the M.S. degree with the Department of Electronics Engineering, Institute of Electronics.

Shiou-Yi Lai received the M.S. degree in electronics engineering from the Department of Electronics Engineering, Institute of Electronics, National Chiao Tung University, Hsinchu, Taiwan, in 2013.

He is currently with the Ministry of the Interior, Taipei, Taiwan.

You-Sheng Liu is currently pursuing the B.S. degree with the Department of Electronics Engineering, National Chiao Tung University, Hsinchu, Taiwan.